



HAL
open science

Selective CO₂ reduction into formate using Ln-Ta oxynitrides combined with a binuclear Ru(II) complex under visible light

Kanemichi Muraoka, Miharuru Eguchi, Osamu Ishitani, François Cheviré,
Kazuhiko Maeda

► **To cite this version:**

Kanemichi Muraoka, Miharuru Eguchi, Osamu Ishitani, François Cheviré, Kazuhiko Maeda. Selective CO₂ reduction into formate using Ln-Ta oxynitrides combined with a binuclear Ru(II) complex under visible light. *Journal of Energy Chemistry*, 2021, 55, pp.176-182. 10.1016/j.jechem.2020.06.064 . hal-02895318

HAL Id: hal-02895318

<https://univ-rennes.hal.science/hal-02895318>

Submitted on 9 Jul 2020

HAL is a multi-disciplinary open access archive for the deposit and dissemination of scientific research documents, whether they are published or not. The documents may come from teaching and research institutions in France or abroad, or from public or private research centers.

L'archive ouverte pluridisciplinaire **HAL**, est destinée au dépôt et à la diffusion de documents scientifiques de niveau recherche, publiés ou non, émanant des établissements d'enseignement et de recherche français ou étrangers, des laboratoires publics ou privés.

Selective CO₂ reduction into formate using Ln-Ta oxynitrides combined with a binuclear Ru(II) complex under visible light

Kanemichi Muraoka^{a,b}, Miharuru Eguchi^c, Osamu Ishitani^{a,*}, François Cheviré^d, Kazuhiko Maeda^{a,*}

^a *Department of Chemistry, School of Science, Tokyo Institute of Technology, Meguro-ku 152-8550, Tokyo, Japan*

^b *Japan Society for the Promotion of Science, Chiyoda-ku 102-0083, Tokyo, Japan*

^c *Research Center for Functional Materials, National Institute for Materials Science, Tsukuba 305-0044, Ibaraki, Japan*

^d *Univ Rennes, CNRS, ISCR-UMR 6226, Rennes F-35000, France*

*Corresponding authors

Email addresses: ishitani@chem.titech.ac.jp (O. Ishitani), maedak@chem.titech.ac.jp (K. Maeda)

KEYWORDS: Artificial photosynthesis; Heterogeneous photocatalysis; Mixed anion compounds; Solar fuels

ABSTRACT

Hybrid materials constructed from a visible-light-absorbing semiconductor and a functional metal complex have attracted attention as efficient photocatalysts for CO₂ reduction with high selectivity to a desired product. In this work, defect fluorite-type Ln-Ta oxynitrides LnTaO_xN_y (Ln = Nd, Sm, Gd, Tb, Dy and Ho) were examined as the semiconductor

component in a hybrid photocatalyst system combined with known Ag nanoparticle promoter and binuclear ruthenium(II) complex (**RuRu'**). Among the LnTaO_xN_y examined, TbTaO_xN_y gave the highest performance for CO_2 reduction under visible light ($\lambda > 400$ nm), with a **RuRu'**-based turnover number of 18 and high selectivity to formate (>99%). Physicochemical analyses indicated that high crystallinity and more negative conduction band potential of LnTaO_xN_y with the absence of Ln-4f states in the band gap structure contributed to higher activity of the hybrid photocatalyst.

1. Introduction

Catalytic conversion of anthropogenic CO_2 into energy rich chemicals with the aid of visible light energy could be a potential means of addressing the shortage of carbon resources and global warming issues [1–8]. Hybrid materials that consist of visible-light-absorbing semiconductors and (photo)catalytically active metal complexes have been reported to function as good photocatalysts for CO_2 reduction under visible light [2,7,8]. For example, a binuclear Ru(II) complex having a photosensitizer and catalyst units in one molecule (**RuRu'**, see Fig. 1) works as an efficient homogeneous photocatalyst for CO_2 reduction, but requires a relatively strong electron donor for operation because of its low photooxidation ability. Combining the **RuRu'** with a visible-light-absorbing semiconductor that has strong oxidation ability enables one to accomplish CO_2 reduction even with the use of a weak electron donor [7]. In some photoelectrochemical systems constructed from a similar binuclear metal complex and a semiconductor, sacrificial reagent-free CO_2 reduction has been achieved [9–11]. As these hybrid systems are based on the combination of photocatalysis of semiconductors and molecules, it is important to develop both of the two in harmony.

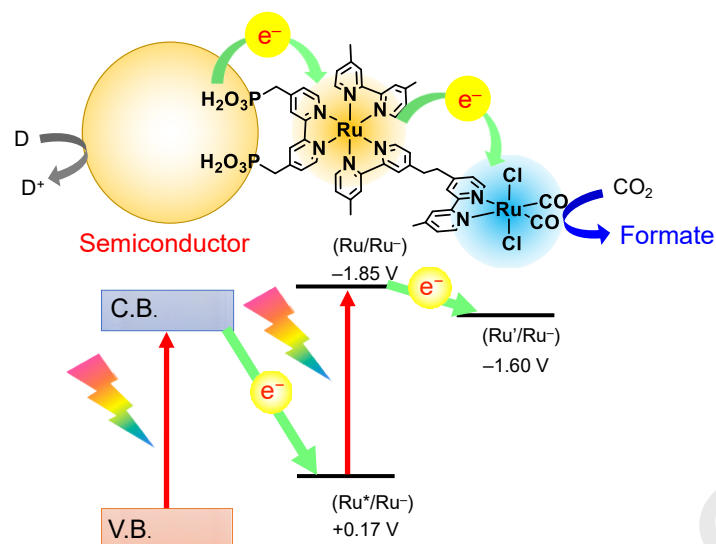


Fig. 1. Hybrid photocatalyst constructed from a visible-light-absorbing semiconductor and a binuclear Ru(II) complex (**RuRu'**).

Focusing on the semiconductor component, various semiconductor materials including TaON [12], Ta₃N₅ [13], GaN:ZnO [14], and Li₂LaTa₂O₆N [15], C/N polymers [16] and Pb₂Ti₂O_{5.4}F_{1.2} [17] have been reported to become active semiconductor components for the Z-scheme CO₂ reduction with the aid of **RuRu'**. It has been also shown that for efficient CO₂ reduction, the potential of the conduction band minimum (CBM) of a semiconductor applied to the Z-scheme system has to be more negative than -1.3 V (vs Ag/AgNO₃), which is equivalent to the excited-state oxidation potential of the photosensitizer unit in **RuRu'**, because suppression of back electron transfer from **RuRu'** to the semiconductor is essential [7]. Although several non-oxide materials have been reported to work as the semiconductor component in the hybrid photocatalyst with **RuRu'** for visible-light-driven CO₂ reduction, it is still important to search for a new semiconductor material for the application.

In heterogeneous photocatalysis for water splitting, rare earth-based semiconductor materials are known to show unique photocatalytic activities, depending on the rare-earth element. Ln-containing oxide semiconductors have been reported to show photocatalytic activities for water splitting under UV irradiation [18–25]. For visible light photocatalysis,

Domen et al. have reported that oxysulfides $\text{Ln}_2\text{Ti}_2\text{S}_2\text{O}_5$ showed activities for H_2 and O_2 evolution half reactions in the presence of an electron donor and an acceptor, respectively [26]. Some Ln-containing transition metal oxynitrides have been shown to act as photocatalysts for the water reduction and/or oxidation half reactions under visible light [27–29]. Visible-light-driven overall water splitting has been accomplished using $\text{LaMg}_x\text{Ta}_{1-x}\text{O}_{1+3x}\text{N}_{2-3x}$ ($x \geq 1/3$) [30]. Thus, there are a lot of examples of Ln-based water splitting photocatalysts. Recently, rare-earth species have been reported as effective modifiers for CO_2 reduction over $\text{Ag}/\text{Ga}_2\text{O}_3$ photocatalyst under UV irradiation [31]. However, there are very few that describe visible-light-driven Z-scheme CO_2 reduction using a Ln-containing semiconductor photocatalyst.

We have previously reported Y-Ta oxynitride with a defect fluorite structure served as an effective semiconductor component in Z-scheme CO_2 reduction to produced formate, with confirmation by isotope tracer experiment using $^{13}\text{CO}_2$ [32]. In this work, we examined Ln-Ta oxynitrides (LnTaO_xN_y ; Ln = Nd, Sm, Gd, Tb, Dy and Ho) as the new candidates for the Z-scheme CO_2 reduction system. The photocatalytic activities were discussed on the basis of the results of physicochemical analyses.

2. Experimental

2.1. Materials and reagents

$\text{Nd}(\text{NO}_3)_3 \cdot 6\text{H}_2\text{O}$ (99.5%), $\text{Sm}(\text{NO}_3)_3 \cdot 6\text{H}_2\text{O}$ (99.5%), $\text{Gd}(\text{NO}_3)_3 \cdot 6\text{H}_2\text{O}$ (99.5%), $\text{Dy}(\text{NO}_3)_3 \cdot 6\text{H}_2\text{O}$ (99.5%), anhydrous citric acid (CA; 98.0%) and I_2 ($\geq 99.8\%$) were purchased from FUJIFILM Wako Pure Chemicals Co. $\text{Tb}(\text{NO}_3)_3 \cdot 6\text{H}_2\text{O}$ (99.9%), TaCl_5 (95%), AgNO_3 (99.8%), ethylene glycol (EG; 99.5%) methanol ($>99.8\%$), acetonitrile (MeCN; $>99.5\%$), triethanolamine (TEOA; $>98.0\%$) and acetone ($\geq 99.5\%$) were purchased from Kanto Chemicals Co. $\text{Ho}(\text{NO}_3)_3 \cdot 5\text{H}_2\text{O}$ (99.5%) were purchased from High Purity Chemicals Co. Tetraethylammonium tetrafluoroborate (Et_4NBF_4 ; 99%) was received from Aldrich Co.

Gases of NH_3 (>99.9995%) and CO_2 (>99.9995%) were purchased from Sumitomo Seika Chemicals Co. and Taiyo Nippon Sanso Co., respectively.

MeCN was distilled over P_2O_5 twice, and then distilled over CaH_2 prior to use. TEOA was distilled under reduced pressure (<1 Torr) and then stored under N_2 prior to use.

2.2. Synthesis of Ln-Ta oxynitrides LnTaO_xN_y

Ln-Ta oxides were synthesized by the polymerized complex (PC) method reported by Kakihana [33]. 0.014 mol of TaCl_5 was dissolved in 100 mL of methanol. Subsequently, 0.21 mol of CA was added to the methanol solution with continuous stirring at room temperature to produce a metal-CA complex. A 0.014 mol quantity of $\text{Ln}(\text{NO}_3)_3$ hydrate was then added to the solution and the mixture was magnetically stirred to make a transparent solution, after which 0.84 mol of EG was added. The resulting mixture was gradually heated to approximately 473 K to remove the methanol and to accelerate the esterification reaction between CA and EG. Upon continued heating, the solution began to gel, eventually transitioning to a glassy, transparent, brownish resin. This resin was thermally decomposed in a heating mantle at 673 K to produce a grey solid, and carbon-based compounds were removed by calcination on an Al_2O_3 plate at 873 K for 2 h to yield a powder. This amorphous Ln-Ta oxide powder was nitrided by heating at 1123 K under a flow of gaseous NH_3 in a tubular furnace [34]. After nitridation, the resulting powder was washed six times with distilled water and dried at 343 K overnight.

2.3. Modification with Ag nanoparticles

The as-prepared LnTaO_xN_y powder was modified with Ag nanoparticles by an impregnation method. 10 mL of an aqueous AgNO_3 solution (containing 1.5 wt% Ag vs. LnTaO_xN_y) was slowly added dropwise into 10 mL of H_2O , in which 100 mg of LnTaO_xN_y was suspended, with continuous stirring. H_2O was subsequently removed from the mixture by distillation under reduced pressure in a rotary evaporator. Finally, the as-obtained powder

was placed in an alumina boat and heated under a flow of H_2 (20 mL min^{-1}) at 473 K for 1 h in a tube furnace.

Our previous studies have shown that the loaded Ag nanoparticles on a visible-light-absorbing semiconductor, which are in the form of nanoparticles of 3–30 nm in size, work as electron traps to facilitate interfacial electron transfer from the semiconductor to the photosensitizing unit of **RuRu'** during Z-scheme CO_2 reduction [16,32,35]. The detailed results and discussion can be found elsewhere.

2.4. Adsorption of **RuRu'** onto Ag-loaded LnTaO_xN_y

The as-prepared $\text{Ag/LnTaO}_x\text{N}_y$ powder (30 mg) was dispersed in 15 mL of MeCN containing **RuRu'** ($3.0 \mu\text{mol g}^{-1}$ vs. $\text{Ag/LnTaO}_x\text{N}_y$). **RuRu'** was synthesized according to our previous report [12]. The suspension was stirred at room temperature in the dark overnight to allow for adsorption/desorption equilibration. The resulting powders were collected by filtration and washed with 5 mL of MeCN or methanol. UV-vis absorption measurements revealed that **RuRu'** quantitatively adsorbed on the surface of $\text{Ag/LnTaO}_x\text{N}_y$. After washing, the powders were dried at room temperature for 3 h under reduced pressure. In our previous studies, this procedure allows one to couple **RuRu'** on the surface of a semiconductor while keeping the structure of **RuRu'** [12,16,17]. It has been confirmed that both Ag and **RuRu'** were necessary to obtaining appreciable formate production [13,16,32,35]. The as-obtained hybrid material was employed as the photocatalyst for the CO_2 reduction reaction.

2.5. Characterization of materials

The prepared materials were characterized using X-ray diffraction (XRD; MiniFlex600, Rigaku, $\text{Cu } K_\alpha$ radiation), UV-vis diffuse reflectance spectroscopy (DRS; V-565, Jasco), and transmission electron microscopy (TEM; H-7650, Hitachi High-Technologies). The Brunauer-Emmett-Teller (BET) surface area was measured using a nitrogen adsorption instrument (BELSOEP-mini II, MicrotracBEL) at liquid-nitrogen temperature.

2.6. Mott-Schottky plot measurements

LnTaO_xN_y electrodes were prepared by electrophoretic deposition on a fluorine-doped tin oxide (FTO) substrate. A pair of FTO glasses were immersed in 50 mL of acetone containing 100 mg of LnTaO_xN_y powder and 10 mg of I_2 . The FTO electrodes were connected to a direct current power supply (GW Instek PSW 80-13.5), to apply a bias of 50 V for 1 min. The LnTaO_xN_y -coated FTO electrode was finally heated at 673 K for 1 h under a N_2 flow in tube furnace.

Mott-Schottky plots were measured in MeCN/TEOA (4/1 v/v) mixed solution containing a 0.1 M Et_4NBF_4 as an electrolyte at room temperature with a potentiostat (BAS ALS/CHI-760e) in a three-electrode system. $\text{LnTaO}_x\text{N}_y/\text{FTO}$ electrodes were used as working electrodes. A Pt wire and a Ag/AgNO_3 electrode were used as the counter and reference electrodes, respectively. Mott-Schottky plots were recorded at a frequency of 100 Hz.

2.7. Photocatalytic CO_2 reduction reaction

8 mg of photocatalyst powder was dispersed in 4 mL of a MeCN/TEOA mixed solution (4:1 v/v) in an 8 mL test tube. The suspension was subsequently purged with CO_2 gas for 20 min prior to irradiation. The light source employed in this work was a 400 W high pressure Hg lamp (SEN) with an aqueous NaNO_2 solution filter to allow for visible light irradiation ($\lambda > 400$ nm). After 15 h of visible light irradiation, the liquid phase of the reaction mixture was analyzed using a capillary electrophoresis system (Otsuka Electronics Co. CAPI-3300) and the gaseous phase of the reaction cell was analyzed with a gas chromatograph (GL science, GC323) employing a thermal conductivity detector (TCD), an activated carbon column and argon as the carrier gas. The selectivity toward formate production during the CO_2 reduction reaction was calculated on the basis of the ratio of formate generated to the total amount of reduction products (i.e., formate, CO, and H_2). Blank tests were performed using the same

photocatalyst suspension but without irradiation. Note that the amount of formate generation reported in this work was calculated by subtracting the blank portion.

The turnover number (TON) for formate production was calculated as:

$$\text{TON} = [\text{Formate}]/[\text{RuRu'}],$$

where [Formate] and [RuRu'] indicate the amounts of formate produced and RuRu' introduced in the hybrid photocatalyst, respectively.

3. Results and discussion

3.1. Synthesis and characterization of LnTaO_xN_y

It is known that the Ln-Ta-O-N system contains several phases such as perovskites, pyrochlores and defect fluorites, depending on the Ln element [34,36]. It has been suggested that LnTaO_xN_y with smaller Ln³⁺ cations prefer to possess defect fluorite structure [34]. The obtained phase is also dependent on the synthesis route. As a crystalline phase, pyrochlore structure has been observed for Ln = Ce → Gd, but the use of soft chemistry route for the precursor synthesis enables to stabilize the defect fluorite type for a wide range of Ln [37].

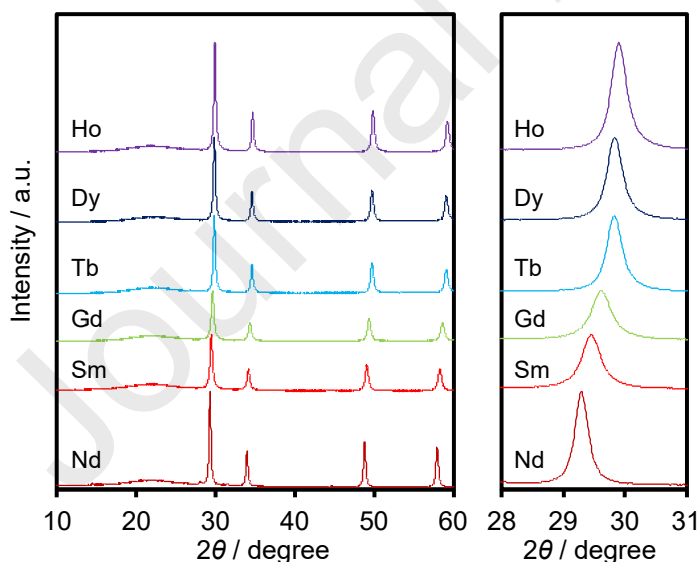


Fig. 2. XRD patterns for the as-synthesized LnTaO_xN_y.

Fig. 2 shows the XRD patterns of the as-synthesized LnTaO_xN_y materials. According to the previous literatures, we deduced that the as-synthesized LnTaO_xN_y had defect fluorite structure as the main phase, except for the Nd specimen that contained several different phases (see Fig. S1). Considering the larger ionic size of Nd^{3+} , the Nd specimen may be pyrochlore (or a mixture with fluorite). As the atomic number increased, the positions of the diffraction peaks successively shifted to higher 2θ angles. This shift is reasonable considering that the ionic radii of Ln^{3+} become smaller with increasing the atomic number due to the lanthanide contraction. A similar peak shift with respect to Ln^{3+} ions has been observed in $\text{Ln}_2\text{Ti}_2\text{S}_2\text{O}_5$ [26]. On the other hand, the full width at half maximum (FWHM) of the diffraction peaks were irregularly changed with respect to Ln^{3+} in LnTaO_xN_y . As listed in Table 1, the FWHM of the 110 reflection is relatively small for $\text{Ln} = \text{Nd, Tb and Ho}$ compared to others, suggesting higher crystallinity of LnTaO_xN_y ($\text{Ln} = \text{Nd, Tb and Ho}$).

Table 1. FWHM, specific surface areas of the as-synthesized LnTaO_xN_y .

Ln	FWHM of the 110 reflection	Specific surface area ($\text{m}^2 \text{g}^{-1}$)	Flat-band potential (V vs. Ag/AgNO_3)
Nd	0.23	14	-1.44
Sm	0.35	15	-1.38
Gd	0.37	15	-1.44
Tb	0.27	14	-1.47
Dy	0.28	14	-1.32
Ho	0.28	14	-1.48

Fig. 3 shows TEM images of the same LnTaO_xN_y materials. All of them consisted of aggregated particles with primary particle sizes that range from several tens of nm to 50 nm, forming larger secondary particles. The specific surface areas of the synthesized LnTaO_xN_y were determined to be 14–15 $\text{m}^2 \text{g}^{-1}$ (Table 1), which is very close to the value of an Y-Ta oxynitride reported previously (16 $\text{m}^2 \text{g}^{-1}$) [32]. Therefore, no significant impact of the lanthanide element on the morphology and the specific surface area was observed.

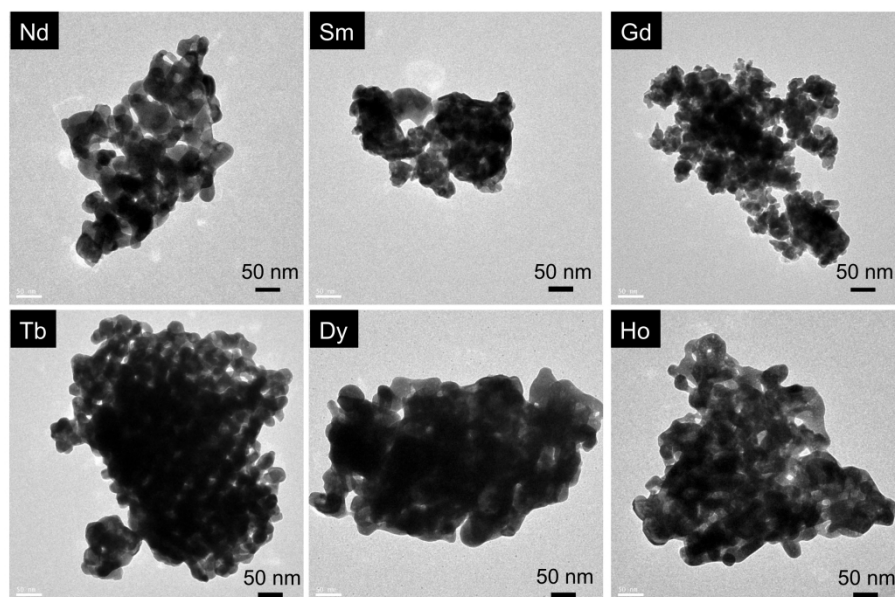


Fig. 3. TEM images for the as-synthesized LnTaO_xN_y .

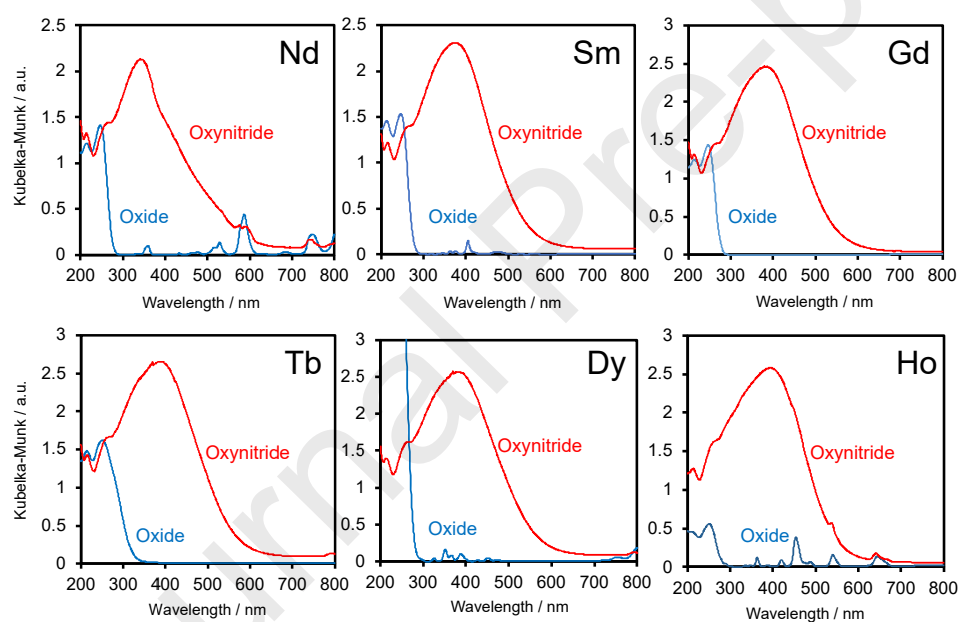


Fig. 4. UV-vis DRS spectra for the as-synthesized LnTaO_xN_y and the corresponding oxide precursors.

3.2. Optical absorption properties and band-edge potentials

UV-vis DRS of LnTaO_xN_y are shown in Figs. 4 and S2, along with their oxide precursors for comparison. The absorption band edges of the precursor oxides appeared at around 300 nm, consistent with the report by Machida et al. on crystalized LnTaO_4 ($\text{Ln} = \text{Nd}$ and Sm)

[20]. Some sharp peaks appearing at wavelengths longer than 300 nm are attributed to f-f transitions derived from Ln^{3+} ions [19–21].

Nitridation of these oxides with dry NH_3 at 1123 K to yield oxynitrides resulted in a significant red-shift of absorption edge caused by the reduction of the band gap, which arises from the N-2p state at the upper part of the valence band in LnTaO_xN_y , as observed in many oxynitride materials [38]. As the atomic number of Ln elements increased, the absorption band edge of LnTaO_xN_y tended to shift to longer wavelengths (Fig. S2), except for the Nd derivative that contained some impurity phases (Fig. S1). An identical trend has been observed in $\text{Ln}_2\text{Ti}_2\text{S}_2\text{O}_5$, in which the O-2p/S-3p/Ln-4f and S-3p/Ln-4f hybridized orbitals in the valence and conduction bands are claimed to cause the red-shift of absorption edge [26]. It should be also noted that LnTaO_xN_y (Ln = Nd, Ho) had characteristic absorption peaks derived from the f-f transitions, indicating that the Ln-4f states existed in the band gap of LnTaO_xN .

Flat-band potential (E_{FB}) is an important parameter of a semiconductor that influences metal-complex/semiconductor hybrid photocatalysts [14]. To determine the E_{FB} values of the as-prepared LnTaO_xN_y , Mott-Schottky plot measurements were conducted. As shown in Fig. 5, all of the Mott-Schottky plots have positive slopes, indicating n-type semiconducting character of LnTaO_xN_y . This should be reasonable, considering the fact that the LnTaO_xN_y compounds having defect fluorite structure contain a considerable number of anionic defects; the formation of anionic vacancies is accompanied by the generation of electrons, which is the origin of n-type semiconductivity. The E_{FB} values were obtained by extrapolation of the linear portion to the x -axis intercept, and were listed in Table 1. The result showed that the values were a little fluctuant with respect to the Ln element, but ranged from -1.5 to -1.3 V vs. Ag/AgNO_3 . The conduction band minimum (CBM) of an n-type semiconductor lies negatively ca. 0.1–0.3 V from the E_{FB} , depending on the conductivity [39]. Therefore, the

CBM values of the LnTaO_xN_y could be estimated to be ca. -1.6 ± 0.2 V, which is similar to or slightly more negative than that reported in Y-Ta oxynitride with the same defect fluorite structure (-1.40 V) [32] and is also negative enough to allow for the forward electron transfer from the semiconductor to the excited state of **RuRu'**, while suppressing the back electron transfer from the excited **RuRu'** [7].

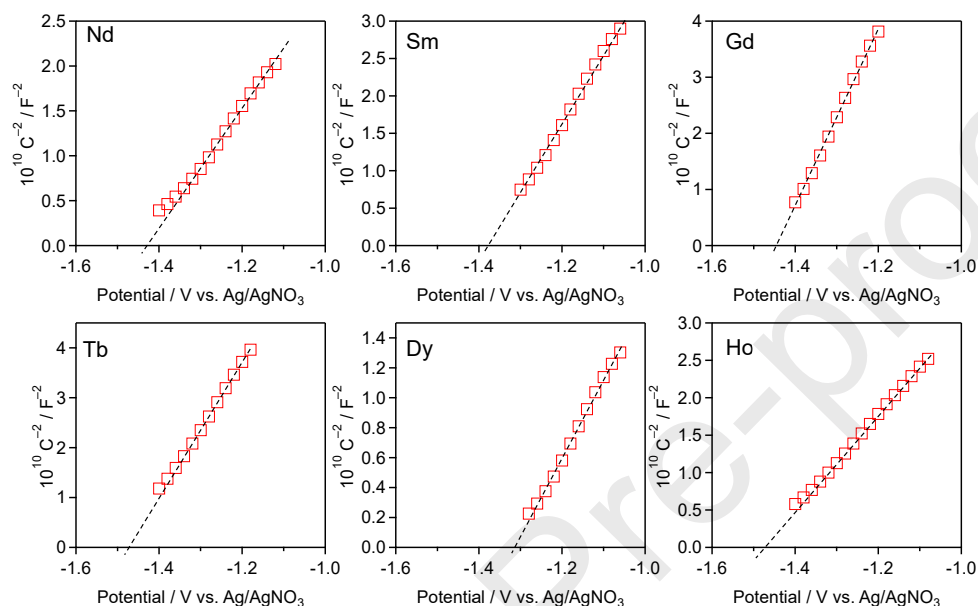


Fig. 5. Mott-Schottky plots for the as-synthesized LnTaO_xN_y .

3.3. Photocatalytic activity

The as-synthesized LnTaO_xN_y materials were tested as the semiconductor components of the hybrid CO_2 photoreduction system with **RuRu'**. CO_2 reduction reaction was conducted in a mixed solution of MeCN and TEOA under visible-light irradiation ($\lambda > 400$ nm), in which TEOA acted as an electron donor to scavenge holes in the valence band of LnTaO_xN_y . As shown in Fig. 6, photocatalytic activities for the CO_2 reduction reaction were strongly dependent on the Ln element. In the cases of Ln = Nd and Sm, no formate was detected. On the other hand, other materials (Ln = Gd, Tb, Dy, and Ho) catalytically produced formate, with TONs greater than 1. Among the LnTaO_xN_y materials tested, the Tb derivative showed the highest activity, which was almost the same level as Y-Ta oxynitride reported before

[32]. These active LnTaO_xN_y materials gave very high selectivity to formate (>99%), with negligible production of other products (e.g., CO or H_2).

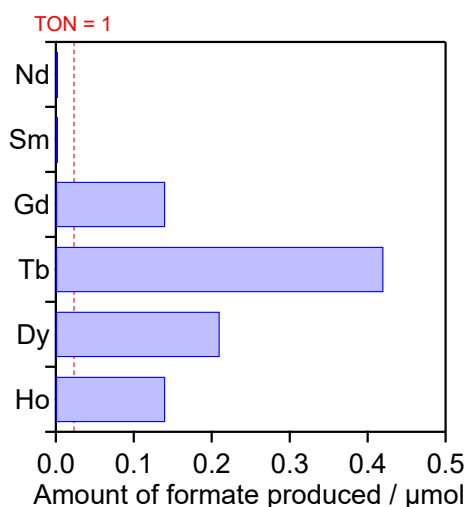


Fig. 6. Photocatalytic activities for CO_2 reduction over **RuRu'**/Ag/ LnTaO_xN_y under visible light ($\lambda > 400$ nm). Reaction conditions: catalyst, 8.0 mg; reactant solution, mixed solution of MeCN and TEOA (4:1 v/v, 4.0 mL); light source, 400 W high-pressure Hg lamp with a K_2CrO_4 aqueous solution filter. Reaction time: 15 h. The dotted red line indicates the level of TON of 1 with respect to **RuRu'**. No reaction took place in the absence of either LnTaO_xN_y or **RuRu'**.

3.4. Factors affecting photocatalytic activity

Thus, it was shown that the photocatalytic activity for the Z-scheme CO_2 reduction using LnTaO_xN_y was strongly influenced by the Ln element in LnTaO_xN_y . To accomplish the reaction, electrons and holes photogenerated in LnTaO_xN_y have to be consumed by reduction and oxidation processes, respectively, while minimizing recombination. It has been reported that the electron-hole recombination in a semiconductor photocatalyst can be minimized by improving the crystallinity of the semiconductor [40,41]. In the present work, the importance of crystallinity could be seen; SmTaO_xN_y and GdTaO_xN_y having lower crystallinity (i.e., greater FWHM, see Table 1) showed relatively low (or negligible) photocatalytic activities

(Fig. 6). The inactivity of the Nd derivative is most likely due to the low quality of the material, as it contained some unreacted Nd impurities (Fig. S1); therefore, electron-hole recombination would be significant.

In addition to crystallinity of semiconductor, it appears that there are some other factors affecting the photocatalytic activity. As listed in Table 1, LnTaO_xN_y ($\text{Ln} = \text{Tb}, \text{Dy}$ and Ho) had similar crystallinity to each other, but showed different activities (Fig. 6). While TbTaO_xN_y and HoTaO_xN_y had almost the same crystallinity and E_{FB} , the former showed three times higher activity than the latter. UV-vis DRS (Fig. 4) showed an obvious contribution of Ln-4f states in the band gap of the lower activity specimen ($\text{Ln} = \text{Ho}$), in contrast to TbTaO_xN_y that showed the highest photocatalytic activity. The existence of Ln-4f states in the band gap of a semiconductor may lead to lower photocatalytic activity because such states can work as effective traps of photogenerated charge carriers, as reported earlier [20].

In the case of NdTaO_xN_y , as compared to TbTaO_xN_y , it is likely that the E_{FB} (in other words, CBM potential) is another important factor that determines the photocatalytic performance of LnTaO_xN_y , in addition to the negative impact of the existence of Ln-4f states in the band gap. In fact, the E_{FB} of NdTaO_xN_y was 0.15 V more positive than that of TbTaO_xN_y , indicating that the reactivity of the photoexcited electron is lower in the former than in the latter. Although one may think that the difference of 0.1–0.2 V is small, it has been reported that such a small difference (0.1–0.2 V) in the CBM potential of semiconductors causes a significant difference in photocatalytic activity for the Z-scheme CO_2 reduction using a visible-light-absorbing semiconductor and **RuRu'** [14].

On the basis of the discussion above, high crystallinity, more negative conduction band potential and the absence of Ln-4f states in the band gap are important factors for LnTaO_xN_y semiconductors showing high photocatalytic activity. Nevertheless, the absolute activity of the present hybrid materials (even for the best-performing one with TbTaO_xN_y) was still very

low, as compared to similar hybrid materials constructed with other non-oxide semiconductors such as TaON or Ta₃N₅. The synthesized TbTaO_xN_y seems to work under longer wavelength visible light (e.g., >500 nm) owing to its extended absorption band (~600 nm), but the TbTaO_xN_y-based hybrid did not work under >500 nm irradiation. This means that improvement of the preparation method for LnTaO_xN_y is necessary, and will be investigated as part of our future works.

4. Conclusions

Hybrid photocatalysts were developed using visible-light-absorbing LnTaO_xN_y (Ln = Nd, Sm, Gd, Tb, Dy and Ho) semiconductors and a Ru(II) binuclear complex for CO₂ reduction under visible light ($\lambda > 400$ nm). Selective reduction of CO₂ into formate was achieved with hybrids consisting of LnTaO_xN_y (Ln = Gd, Tb, Dy and Ho) in MeCN containing TEOA as an electron donor. The highest activity was obtained with the Tb derivative. The use of LnTaO_xN_y with high crystallinity and more negative conduction band potential, while avoiding participation of Ln-4f states in the band gap structure, was found to be essential to attaining high photocatalytic activity. We believe that the knowledge obtained in this work will be useful for designing a new semiconductor material not only for the Z-scheme CO₂ reduction with a supramolecular complex but also for a system combined with a molecular catalyst, because semiconductor photocatalysis is common in both systems.

Supporting Information. Additional characterization data. This material is available free of charge via the Internet.

ACKNOWLEDGMENTS

This work was supported by a Grant-in-Aid for Scientific Research on Innovative Area “Mixed Anion (Projects JP16K21724 and JP16H06441)” from the Japan Society for the

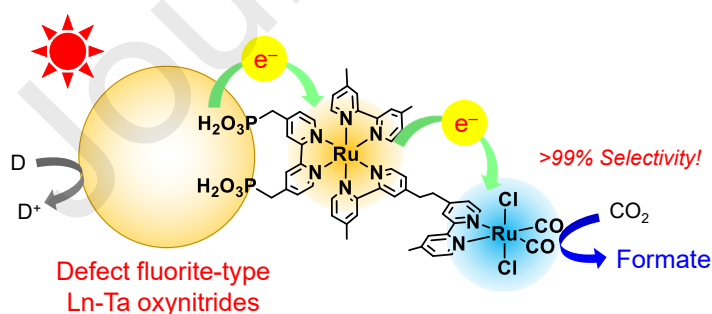
Promotion of Science (JSPS) and a CREST program (Project JPMJCR13L1) from the Japan Science and Technology Agency (JST). K. Muraoka wishes to acknowledge support in the form of a JSPS Fellowship for Young Scientists (Project JP17J06914).

REFERENCES

- [1] E.E. Benson, C.P. Kubiak, A.J. Sathrum, J.M. Smieja, *Chem. Soc. Rev.* 38 (2009) 89–99.
- [2] S. Sato, T. Arai, T. Morikawa, *Inorg. Chem.* 54 (2015) 5105–5113.
- [3] Y. Yamazaki, H. Takeda, O. Ishitani, *J. Photochem. Photobiol., C* 25 (2015) 106–137.
- [4] G. Zhang, Z.-A. Lan, X. Wang, *ChemCatChem* 7 (2015) 1422–1423.
- [5] Y. Amao, *Sustainable Energy Fuels* 2 (2018) 1928–1950.
- [6] Y. Fang, X. Wang, *Chem. Commun.* 54 (2018) 5674–5687.
- [7] K. Maeda, *Adv. Mater.*, 31 (2019) 1808205.
- [8] K.E. Dalle, J. Warnan, J.J. Leung, B. Reuillard, I.S. Karmel, E. Reisner, *Chem. Rev.* 119 (2019) 2752–2875.
- [9] G. Sahara, H. Kumagai, K. Maeda, N. Kaeffer, V. Artero, M. Higashi, R. Abe, O. Ishitani, *J. Am. Chem. Soc.* 138 (2016) 14152–14158.
- [10] H. Kumagai, G. Sahara, K. Maeda, M. Higashi, R. Abe, O. Ishitani, *Chem. Sci.* 8 (2017) 4242–4249.
- [11] A. Nakada, T. Uchiyama, N. Kawakami, G. Sahara, S. Nishioka, R. Kamata, H. Kumagai, O. Ishitani, Y. Uchimoto, K. Maeda, *ChemPhotoChem* 3 (2019) 37–45.
- [12] K. Sekizawa, K. Maeda, K. Domen, K. Koike, O. Ishitani, *J. Am. Chem. Soc.* 135 (2013) 4596–4599.
- [13] K. Muraoka, T. Uchiyama, D. Lu, Y. Uchimoto, O. Ishitani, K. Maeda, *Bull. Chem. Soc. Jpn.* 92 (2019) 124–126.
- [14] A. Nakada, R. Kuriki, K. Sekizawa, S. Nishioka, J.J.M. Vequizo, T. Uchiyama, N. Kawakami, D. Lu, A. Yamakata, Y. Uchimoto, O. Ishitani, K. Maeda, *ACS Catal.* 8 (2018) 9744–9754.
- [15] T. Oshima, T. Ichibha, K.S. Qin, K. Muraoka, J.J.M. Vequizo, K. Hibino, R. Kuriki, S. Yamashita, K. Hongo, T. Uchiyama, K. Fujii, D. Lu, R. Maezono, A. Yamakata, H. Kato, K. Kimoto, M. Yashima, Y. Uchimoto, M. Kakihana, O. Ishitani, H. Kageyama, K. Maeda, *Angew. Chem. Int. Ed.* 57 (2018) 8154–8158.
- [16] R. Kuriki, H. Matsunaga, T. Nakashima, K. Wada, A. Yamakata, O. Ishitani, K. Maeda, *J. Am. Chem. Soc.* 138 (2016) 5159–5170.
- [17] R. Kuriki, T. Ichibha, K. Hongo, D. Lu, R. Maezono, H. Kageyama, O. Ishitani, K. Oka, K. Maeda, *J. Am. Chem. Soc.* 140 (2018) 6648–6655.
- [18] A. Kudo, H. Okutomi, H. Kato, *Chem. Lett.* 29 (2000) 1212–1213.
- [19] M. Machida, J.-i. Yabunaka, T. Kijima, *Chem. Mater.* 12 (2000) 812–817.
- [20] M. Machida, S. Murakami, T. Kijima, S. Matsushima, M. Arai, *J. Phys. Chem. B* 105 (2001) 3289–3294.
- [21] M. Machida, J.-i. Yabunaka, T. Kijima, S. Matsushima, M. Arai, *Int. J. Inorg. Mater.* 3 (2001) 545–550.
- [22] R. Abe, M. Higashi, Z. Zou, K. Sayama, Y. Abe, *Chem. Lett.* 33 (2004) 954–955.
- [23] R. Abe, M. Higashi, Z. Zou, K. Sayama, Y. Abe, H. Arakawa, *J. Phys. Chem. B* 108 (2004) 811–814.
- [24] R. Abe, M. Higashi, K. Sayama, Y. Abe, H. Sugihara, *J. Phys. Chem. B* 110 (2006) 2219–2226.

- [25] M. Higashi, R. Abe, H. Sugihara, K. Domen, *Bull. Chem. Soc. Jpn.* 81 (2008) 1315–1321.
- [26] A. Ishikawa, T. Takata, T. Matsumura, J.N. Kondo, M. Hara, H. Kobayashi, K. Domen, *J. Phys. Chem. B* 108 (2004) 2637–2642.
- [27] K. Kawashima, M. Hojamberdiev, H. Wagata, E. Zahedi, K. Yubuta, K. Domen, K. Teshima, *J. Catal.* 344 (2016) 29–37.
- [28] A.P. Black, H. Suzuki, M. Higashi, C. Frontera, C. Ritter, C. De, A. Sundaresan, R. Abe, A. Fuertes, *Chem. Commun.* 54 (2018) 1525–1528.
- [29] H. Wakayama, K. Hibino, K. Fujii, T. Oshima, K. Yanagisawa, Y. Kobayashi, K. Kimoto, M. Yashima, K. Maeda, *Inorg. Chem.* 58 (2019) 6161–6166.
- [30] C. Pan, T. Takata, M. Nakabayashi, T. Matsumoto, N. Shibata, Y. Ikuhara, K. Domen, *Angew. Chem. Int. Ed.* 54 (2015) 2955–2959.
- [31] H. Tatsumi, K. Teramura, Z. Huang, Z. Wang, H. Asakura, S. Hosokawa, T. Tanaka, *Langmuir* 33 (2017) 13929–13935.
- [32] K. Muraoka, H. Kumagai, M. Eguchi, O. Ishitani, K. Maeda, *Chem. Commun.* 52 (2016) 7886–7889.
- [33] M. Kakihana, *J. Sol-Gel Sci. Technol.* 6 (1996) 7–55.
- [34] P. Maillard, F. Tessier, E. Orhan, F. Cheviré, R. Marchand, *Chem. Mater.* 17 (2005) 152–156.
- [35] F. Yoshitomi, K. Sekizawa, K. Maeda, O. Ishitani, *ACS Appl. Mater. Interfaces* 7 (2015) 13092–13097.
- [36] S. Kikkawa, T. Takeda, A. Yoshiasa, P. Maillard, F. Tessier, *Mater. Res. Bull.* 43 (2008) 811–818.
- [37] E. Ray, F. Tessier, F. Cheviré, *Solid State Sci.* 13 (2011) 1031–1035.
- [38] H. Kageyama, K. Hayashi, K. Maeda, J.P. Attfield, Z. Hiroi, J.M. Rondinelli, K.R. Poeppelmeier, *Nat. Commun.* 9 (2018) 772.
- [39] Y. Matsumoto, *J. Solid State Chem.* 126 (1996) 227–234.
- [40] A. Yamakata, T.-a. Ishibashi, H. Kato, A. Kudo, H. Onishi, *J. Phys. Chem. B* 107 (2003) 14383–14387.
- [41] A. Yamakata, H. Yeilin, M. Kawaguchi, T. Hisatomi, J. Kubota, Y. Sakata, K. Domen, *J. Photochem. Photobiol., A* 313 (2015) 168–175.

Graphical abstract



Ln-Ta oxynitrides with defect fluorite structure were found to serve as effective semiconductor components in visible-light-driven Z-scheme CO₂ reduction with a binuclear Ru(II) complex, giving high selectivity to formate (>99%).

Highlights.

- Ln-Ta oxynitrides LnTaO_xN_y (Ln = Nd, Sm, Gd, Tb, Dy and Ho) were synthesized.
- Some of LnTaO_xN_y loaded with Ag and a Ru(II) complex photocatalyzed CO_2 reduction.
- The highest activity was obtained with TbTaO_xN_y .
- High formate selectivity (>99%) was accomplished.

Journal Pre-proofs